Acta Cryst. (1999). A**55**, 1038–1048

Electron density in ammonium dihydrogen phosphate: non-uniqueness of the multipolar model in simple inorganic structures

N. Pérès, A. Boukhris,‡ M. Souhassou, G. Gavoille† and C. Lecomte*

Laboratoire de Cristallographie et Modélisation des Matériaux Minéraux et Biologiques, UPRESA CNRS 7036, Faculté des Sciences, Université Henri Poincaré, Nancy 1, BP 239, 54506 Vandoeuvre-lès-Nancy CEDEX, France. E-mail: lecomte@lcm3b.u-nancy.fr

(*Received 24 December 1998; accepted 27 July 1999*)

Abstract

X-ray and neutron diffraction data of a single crystal of ammonium dihydrogen phosphate have been used for the determination of the electron density using multipolar expansion of the density around each nucleus. As the ammonium group was found to be nearly neutral from unconstrained multipole refinement, constrained refinements have been performed with the charge of the ammonium group ranging from zero to one. On the other hand, the expansion of the radial functions of the phosphorus atom was varied. All refinements led to almost the same agreement factors and residual densities. The consequences of such uncertainties on the topology of the electron density are discussed, namely the topology of the P—O bond critical point.

1. Introduction

The chemical bonds in molecules and crystals may be classified from the knowledge of the topology of the electron density and physical quantities such as atomic charges, and multipole moments may be calculated by integration over the 'atomic basins' (Bader, 1990; Souhassou & Blessing, 1999). The stability of the structure may also be tackled from the competition between different critical points where the gradient of the electron density vanishes (Bader, 1990). All of this justifies the studies that are devoted to accurate experimental determination of the electron density for those crystals for which *ab initio* calculations are still not reliable enough. Two methods can be used for the determination of the electron density: the maximum-entropy method (Roversi *et al.*, 1998) and the multipole expansion (Stewart, 1969); the multipole model is the most suitable for topological analysis. In the present work, we have used the Hansen–Coppens model (Hansen & Coppens, 1978), which uses an expansion of the electron density around each nucleus as:

$$\rho_{\rm at}(r) = \rho_c(r) + P_v\kappa^3\rho_v(\kappa r) + \sum_{l=0}^{l_{\max}}\sum_{m=0}^{l}\kappa'^3 R_{n_l}(\kappa' r)P_{lm\pm}y_{lm\pm}(\theta,\varphi), \quad (1)$$

where ρ_c and ρ_v are spherically averaged Hartree–Fock core and valence densities, $y_{lm\pm}$ are spherical harmonic angular functions in real form.

$$R_{n_l}(\kappa' r) = N_{n_l}R^n\exp(-\kappa'\xi r) \quad (2)$$

are Slater-type radial functions, κ and κ' are the expansion–contraction parameters and P_v and $P_{lm\pm}$ the population parameters.

We report here on the problems encountered when analysing the electron density in ammonium dihydrogen phosphate (ADP) with the simple chemical formula $NH_4H_2PO_4$. One of our interests is the study of the hydrogen bonds that hinder the rotation of the NH_4^+ ion in the crystal (Boukhris, 1995; Boukhris *et al.*, 1994, 1998). On the other hand, ADP shows a phase transition at 148 K from a paraelectric phase at high temperature (space group $I\bar{4}2d$) to an antiferroelectric phase at low temperature (space group $P2_12_12_1$) (Keeling & Pepinsky, 1955). Consequently, by performing the analysis slightly above the transition temperature, we hope to get some insight into the mechanism of the phase transition from the study of the stability (or instability) of the high-temperature phase. In the course of the refinement, and for such a system, we have noticed a very unusual non-uniqueness of the multipole expansion. Non-uniqueness itself is not surprising because some of the parameters are obtained through a nonlinear fitting procedure that can leave multiple solutions and similar statistical accuracy giving rise to highly correlated parameters (Prince & Boggs, 1992; El Haouzi *et al.*, 1996; Kuntzinger *et al.*, 1998, and references therein). To be more explicit, significant variations of the parameters in equation (1) fit the data equally well within accuracy. We have concentrated our attention on the net charge of the ammonium ion, which is correlated to the valence-shell expansion–contraction κ parameters, and on the multipolar radial function κ' parameter of phosphorus. Most solutions may be

‡ Permanent address: Département de Physique, University of Agadir, Morocco.
† Deceased January 1999.

Table 1. *Crystal data used for X-ray experiment*

Formula	$NH_4H_2PO_4$
Space group	$I\bar{4}2d$
Molecular weight	115.03 g mol^{-1}
Radiation, λ	Mo $K\alpha$, 0.7107 Å
Cell parameters (T = 158 K)	a = 7.4700 (5), c = 7.5351 (14) Å
Cell volume	420.5 (1) Å^3
Crystal volume	0.0107 mm^3
Density	ρ_{cal} = 1.81 g cm^{-3}
Absorption coefficient	μ = 0.52 mm^{-1}

disregarded on chemical and physical grounds, and therefore in order to find the significant solution one may generally resort to additional knowledge not given explicitly by the experimental data. On the other hand, if the nature of the critical points and the corresponding electron density do not depend on the solution within the accuracy of the data, the derivatives of the electron density and the Laplacian may be very sensitive to small changes of some parameters of the multipole expansion in such a way that the topology of the electron density cannot be unambiguously fully defined.

2. Experimental

Both neutron and X-ray diffraction experiments have been carried out on single crystals at 158 K, *i.e.* 10 K above the transition temperature. The experimental details of the neutron diffraction experiment may be found in Pérès *et al.* (1997), details of the crystal structure in Boukhris *et al.* (1994) and Boukhris (1995).

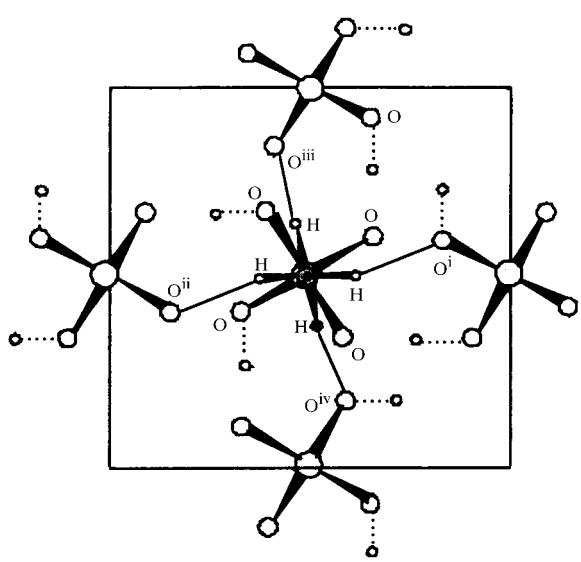

Fig. 1. Projection in the (001) plane of PO_4 and NH_4 tetrahedra showing the strongest N—H···O$_n$ and O—H$_P$—O hydrogen bonds. (i) $\frac{1}{2}+x$, $\bar{y}$, $\frac{3}{4}-z$; (ii) $-\frac{1}{2}+x$, $\bar{y}$, $\frac{3}{4}-z$; (iii) $\bar{x}$, $\frac{1}{2}+y$, $\frac{1}{4}-z$; (iv) $\bar{x}$, $-\frac{1}{2}+y$, $\frac{1}{4}-z$.

Table 2. *Positional and thermal displacement parameters (Å^2) and Gram–Charlier coefficients (Å^3 and Å^4, respectively, for c_{ijk} and d_{ijkl}); estimated errors are given in parentheses*

Atom	Parameter	Value
N	U_{11}	0.0172 (3)
	U_{33}	0.0100 (4)
P	U_{11}	0.0072 (3)
	U_{33}	0.0114 (6)
O	x	0.1477 (1)
	y	0.0847 (1)
	z	0.1150 (1)
	U_{11}	0.0116 (3)
	U_{22}	0.0096 (3)
	U_{33}	0.0159 (3)
	U_{12}	0.0017 (3)
	U_{13}	−0.0057 (3)
	U_{23}	−0.0034 (3)
H_P	x	0.1443 (4)
	y	0.2500
	z	0.125
	U_{11}	0.023 (1)
	U_{22}	0.040 (2)
	U_{33}	0.023 (1)
	U_{12}	–
	U_{13}	–
	U_{23}	0.001 (1)
	c_{123}	0.021 (6)
	d_{2222}	−0.016 (1)
	d_{2223}	−0.021 (3)
H_N	x	0.1085 (8)
	y	0.0161 (4)
	z	0.5768 (4)
	U_{11}	0.054 (2)
	U_{22}	0.034 (1)
	U_{33}	0.041 (1)
	U_{12}	0.004 (1)
	U_{13}	−0.023 (2)
	U_{23}	−0.004 (2)
	c_{111}	−0.016 (3)
	c_{222}	–
	c_{122}	−0.011 (3)
	c_{113}	0.016 (4)
	c_{123}	0.011 (5)
	d_{1113}	0.019 (5)
	d_{1233}	−0.016 (7)
	d_{2223}	0.005 (3)

Crystal data used for X-ray diffraction are given in Table 1. The structure of ADP consists of phosphate groups PO_4 connected by hydrogen bonds and forming octahedra in which the ammonium ions are located. In the paraelectric phase studied here, there are one P and one N atoms in the asymmetric unit located on centers (0, 0, 0) and (0, 0, 1/2); the resulting P—O bonds are therefore equivalent and tetrahedrically arranged. As a consequence, the H_P hydrogen atom lies on the twofold axis (x, 1/4, 1/8) in the middle of O···O lines. Each ammonium hydrogen atom H_N forms three centered or bifurcated hydrogen bonds with two O atoms, one nearest neighbor O$_n$ and one next-nearest neighbour O$_{nn}$ (Fig. 1) (Pérès *et al.*, 1997).

Table 3. *Residual indices and multipole parameters for the different atoms versus the ammonium charge; estimated errors are given in parentheses*

		NH_4 charge				
		+0.1 (2)	+0.3	+0.5	+0.7	+1.0
Atom	Parameter					
N	κ	1.019 (3)	1.017 (3)	1.017 (3)	1.014 (3)	1.009 (3)
	κ'	0.76 (2)	0.76 (2)	0.76 (2)	0.76 (2)	0.76 (2)
	P_v	1.28 (2)	1.29 (2)	1.30 (2)	1.31 (2)	1.30 (2)
	P_{20}	0.000 (8)	−0.001 (8)	−0.001 (8)	−0.001 (8)	−0.001 (7)
	P_{32+}	0.10 (1)	0.096 (9)	0.096 (9)	0.097 (9)	0.100 (9)
	P_{32-}	0.17 (3)	0.17 (3)	0.17 (3)	0.17 (3)	0.16 (3)
	P_{40}	−0.02 (1)	−0.02 (1)	−0.02 (1)	−0.01 (1)	−0.02 (1)
	P_{44+}	0.02 (1)	0.02 (1)	0.02 (1)	0.02 (1)	0.02 (1)
	P_{44-}	0.04 (2)	0.04 (2)	0.05 (2)	0.05 (2)	0.05 (2)
P	κ	1.018 (7)	1.016 (7)	1.013 (7)	1.011 (7)	1.012 (7)
	κ'	1.25 (2)	1.26 (2)	1.28 (2)	1.29 (2)	1.31 (2)
	P_v	1.06 (3)	1.07 (3)	1.09 (3)	1.10 (3)	1.11 (3)
	P_{20}	−0.035 (7)	−0.03 (7)	−0.037 (7)	−0.037 (7)	−0.037 (6)
	P_{32+}	0.061 (6)	0.059 (5)	0.058 (5)	0.057 (5)	0.054 (5)
	P_{32-}	0.22 (3)	0.22 (3)	0.21 (3)	0.21 (3)	0.20 (3)
	P_{40}	−0.030 (6)	−0.029 (6)	−0.028 (6)	−0.028 (6)	−0.027 (5)
	P_{44+}	−0.012 (5)	−0.011 (5)	−0.011 (4)	−0.011 (4)	−0.010 (4)
	P_{44-}	−0.027 (6)	0.027 (6)	0.026 (6)	0.025 (5)	0.023 (5)
O	κ	0.984 (1)	0.984 (1)	0.984 (1)	0.983 (1)	0.982 (1)
	κ'	1.17 (5)	1.16 (5)	1.16 (5)	1.16 (5)	1.18 (5)
	P_v	6.37 (2)	6.38 (2)	6.39 (2)	6.40 (2)	6.43 (2)
	P_{11+}	−0.009 (5)	−0.009 (5)	−0.008 (5)	−0.008 (5)	−0.007 (4)
	P_{11-}	−0.039 (6)	−0.039 (6)	−0.039 (6)	−0.039 (6)	−0.038 (6)
	P_{10}	−0.030 (5)	−0.031 (4)	−0.031 (5)	−0.030 (5)	−0.029 (4)
	P_{20}	0.011 (5)	0.011 (5)	0.011 (5)	0.010 (5)	0.010 (4)
	P_{21+}	−0.005 (5)	−0.005 (5)	−0.005 (5)	−0.005 (5)	−0.006 (4)
	P_{21-}	0.012 (6)	0.013 (6)	0.013 (6)	0.013 (6)	0.012 (6)
	P_{22+}	−0.008 (6)	−0.008 (6)	−0.008 (6)	−0.008 (6)	−0.007 (6)
	P_{22-}	0.015 (5)	0.015 (5)	0.015 (5)	0.015 (5)	0.014 (5)
	P_{30}	0.004 (6)	0.004 (6)	0.004 (6)	0.004 (6)	0.003 (6)
	P_{31+}	−0.021 (7)	−0.020 (7)	−0.019 (7)	−0.018 (7)	−0.017 (7)
	P_{31-}	−0.007 (8)	−0.008 (9)	−0.010 (9)	−0.010 (9)	−0.012 (9)
	P_{32+}	−0.019 (8)	0.020 (8)	0.021 (8)	0.022 (8)	0.023 (8)
	P_{32-}	0.002 (7)	0.002 (7)	0.001 (7)	0.001 (7)	0.000 (7)
	P_{33+}	−0.018 (9)	−0.019 (9)	−0.020 (9)	−0.021 (9)	−0.022 (9)
	P_{33-}	−0.021 (6)	−0.021 (6)	−0.020 (6)	−0.021 (6)	−0.020 (6)
H_P	κ	1.04 (2)	1.00 (2)	0.99 (2)	0.96 (2)	0.93 (2)
	κ'	0.95 (3)	0.94 (2)	0.95 (2)	0.96 (3)	0.96 (2)
	P_v	0.34 (2)	0.37 (2)	0.39 (2)	0.41 (2)	0.44 (2)
	P_{11+}	−0.03 (1)	−0.04 (1)	−0.04 (1)	−0.04 (1)	−0.04 (1)
	P_{20}	−0.09 (1)	−0.09 (1)	−0.09 (1)	−0.09 (1)	−0.09 (1)
	P_{21-}	−0.01 (2)	−0.01 (2)	−0.01 (2)	−0.01 (2)	−0.013 (2)
	P_{22+}	−0.29 (3)	−0.30 (3)	−0.30 (3)	−0.29 (3)	−0.29 (3)
H_N	κ	1.02 (1)	1.04 (1)	1.08 (2)	1.11 (2)	1.15 (2)
	κ'	1.26 (6)	1.31 (6)	1.31 (6)	1.31 (7)	1.31 (7)
	P_v	0.94 (4)	0.88 (2)	0.83 (2)	0.77 (2)	0.70 (2)
	P_{11+}	0.13 (2)	0.12 (1)	0.11 (1)	0.11 (1)	0.10 (1)
	P_{11-}	−0.00 (2)	0.00 (1)	0.00 (1)	0.00 (1)	0.00 (1)
	P_{10}	0.04 (3)	0.03 (3)	0.04 (3)	0.04 (3)	0.04 (3)
	P_{20}	−0.00 (2)	0.00 (2)	0.00 (2)	0.01 (2)	0.01 (2)
	P_{21+}	0.02 (3)	0.02 (3)	0.02 (3)	0.02 (3)	0.03 (3)
	P_{21-}	−0.01 (3)	−0.01 (3)	−0.02 (3)	−0.02 (3)	−0.02 (3)
	P_{22+}	0.07 (3)	0.06 (2)	0.06 (2)	0.06 (2)	0.06 (2)
	P_{22-}	0.01 (2)	0.01 (2)	0.01 (2)	0.01 (2)	0.02 (2)
Scale factor		1.743 (1)	1.743 (1)	1.742 (1)	1.742 (1)	1.742 (1)
Extinction		1.31 (6)	1.31 (6)	1.30 (6)	1.30 (6)	1.28 (6)
Residual factors						
GOF		0.99	0.99	0.99	0.99	0.99
$R(F)$ (%)		0.80	0.80	0.80	0.80	0.80
$wR(F)$ (%)		0.87	0.87	0.87	0.87	0.87

Table 4. *Atomic charges as derived from multipole refinement versus the constrained NH_4 charge*

NH_4 charge	Parameter	N	P	O	H_P	H_N
+0.1 (2)	κ	1.019 (3)	1.018 (7)	0.984 (1)	1.04 (2)	1.02 (1)
	P_v	1.28 (2)	1.06 (3)	6.37 (2)	0.34 (2)	0.94 (4)
	Charge	−0.12 (4)	+0.76 (6)	−0.37 (4)	+0.32 (4)	+0.06 (8)
+0.3	κ	1.017 (3)	1.016 (7)	0.984 (1)	1.00 (2)	1.04 (1)
	P_v	1.29 (2)	1.07 (3)	6.38 (2)	0.37 (2)	0.88 (2)
	Charge	−0.16 (4)	+0.74 (6)	−0.38 (4)	+0.26 (4)	+0.12 (4)
+0.5	κ	1.017 (3)	1.013 (7)	0.984 (1)	0.99 (2)	1.08 (2)
	P_v	1.30 (2)	1.09 (3)	6.39 (2)	0.39 (2)	0.831 (2)
	Charge	−0.18 (4)	+0.66 (6)	−0.39 (4)	+0.23 (4)	+0.17 (4)
+0.7	κ	1.014 (3)	1.011 (7)	0.983 (1)	0.96 (2)	1.11 (2)
	P_v	1.31 (2)	1.10 (3)	6.40 (2)	0.41 (2)	0.77 (1)
	Charge	−0.22 (4)	+0.62 (6)	−0.40 (4)	+0.19 (4)	+0.23 (4)
1.0	κ	1.009 (3)	1.012 (7)	0.982 (1)	0.93 (2)	1.15 (2)
	P_v	1.30 (2)	1.11 (3)	6.43 (2)	0.44 (2)	0.70 (2)
	Charge	−0.21 (4)	+0.54 (6)	−0.43 (4)	+0.12 (4)	+0.30 (4)

2.1. *X-ray data collection*

For X-ray experiments, small single crystals were grown from a supersaturated aqueous solution by slow evaporation at room temperature. The crystal used is prismatic with lateral dimensions 0.25 × 0.21 mm. The distances between the corresponding terminal faces range from 0.24 to 0.27 mm. The X-ray source was graphite-monochromated Mo $K\alpha$ radiation from a sealed tube. Measurements were made on an Enraf–Nonius CAD-4 diffractometer equipped with a nitrogen jet-stream low-temperature system (Soterem N-jet) installed in a dry box to prevent ice formation on the crystal; the gas-stream temperature was monitored to 158±1 K at the crystal. The lattice parameters were obtained from 25 reflections randomly located in the reciprocal space at high 2θ angles. Intensity data were recorded as ω–2θ scan profiles to a resolution of $(\sin\theta/\lambda)_{max} = 1.32$ Å^{-1} for 2376 reflections ($0 < h < 19$, $0 < k < 19$, $0 < l < 19$). During the data collection, four standard reflections, 062, 800, 085 and 095, were measured at 2 h intervals. The total scan width ($\Delta\omega$) was $1 + 0.35\tan\theta$ with a fixed horizontal and vertical detector aperture of 3 × 6 mm. The scan speed $\nu = \mathrm{d}\omega/\mathrm{d}t$ ranged from 1.26 to 2.75 min^{-1}. The total X-ray exposure time was 67 h.†

2.2. *X-ray data processing*

Data reduction was carried out with the *DREAR* programs (Blessing, 1987). Reflection integration limits were taken from a Gaussian model of the peak-width variations. A polynomial fit to the decay of the standard reflection intensities was applied to scale the data and derive the instrumental instability coefficient ($\langle P\rangle = 0.0077\%$). The absorption corrections were performed using the *ABSORB* program (De Titta, 1985). Averaging the equivalent reflections led to the internal agreement factors $R_1(I) = 1.22$, $R_2(I) = 1.36$ and $wR(I) = 2.26\%$ for 2376 measured intensities giving rise to 923 unique reflections. These internal agreement factors demonstrate the excellent quality of the data used for this critical analysis of charge-density refinement results.

2.3. *Multipole refinements*

Position and mean-square displacement parameters of non-H atoms were refined at high order (HO) ($0.8 < \sin\theta/\lambda < 1.32$ Å^{-1}) from X-ray diffraction data (Table 2) (Boukhris, 1995). The positions of the ammonium H atoms were determined from the neutron diffraction experiment and the hydrogen linked to the phosphate O atoms (H_P) was fixed at the special position (x, 1/4, 1/8) (Pérès *et al.*, 1997). The hydrogen thermal displacement parameters $U(X–N)$ were calculated from the neutron data $U(N)$ as:

$$\begin{aligned} U^{ii}(X-N) &= U^{ii}(N) + \Delta U^{ii} \\ U^{ij}(X-N) &= U^{ij}(N) \quad \text{for } i \neq j, \end{aligned} \tag{3}$$

where ΔU^{ii} is the average of the observed difference between U^{ii} values obtained from the HO X-ray refinement and neutron diffraction for the heavy atoms (P, O, N). The anharmonic contributions of the protons obtained from the neutron diffraction experiment (Table 2) were also included in the refinement as fixed parameters.

The initial n_l and ξ parameters of the phosphorus atom are difficult to select and were chosen according to our previous works on L-arginine phosphate (Espinosa *et al.*, 1996) and on phosphoric acid (Moss *et al.*, 1995; Souhassou *et al.*, 1995): $n_l = 6, 6, 6, 6$ for $l = 1$ to 4 and $\xi = 3.6$ Bohr^{-1} (Bohr radius = 0.529×10^{-10} m).

The X-ray data up to $\sin\theta/\lambda = 1$ Å^{-1} (474 reflections) have been used in the refinements of the electron-

† Lists of structure factors have been deposited and are available from the IUCr electronic archives (Reference: AU0165). Services for accessing these data are described at the back of the journal.

density parameters. Using data collected at larger diffraction angles, *i.e.* up to 1.32 $\AA^{-1}$, introduced more noise in the electron-density maps than realistic features, owing to the loss of accuracy of the measurement of the intensities at large angles with conventional diffractometers.

The refinement of the electron density [equations (1) and (2)] was performed according to the following procedure:

(*a*) Scale factor, the x, y, z, U^{ij} being fixed from HO (P, O, N atoms) and $X-N$ (H atoms) refinements.

(*b*) Secondary extinction of type I.

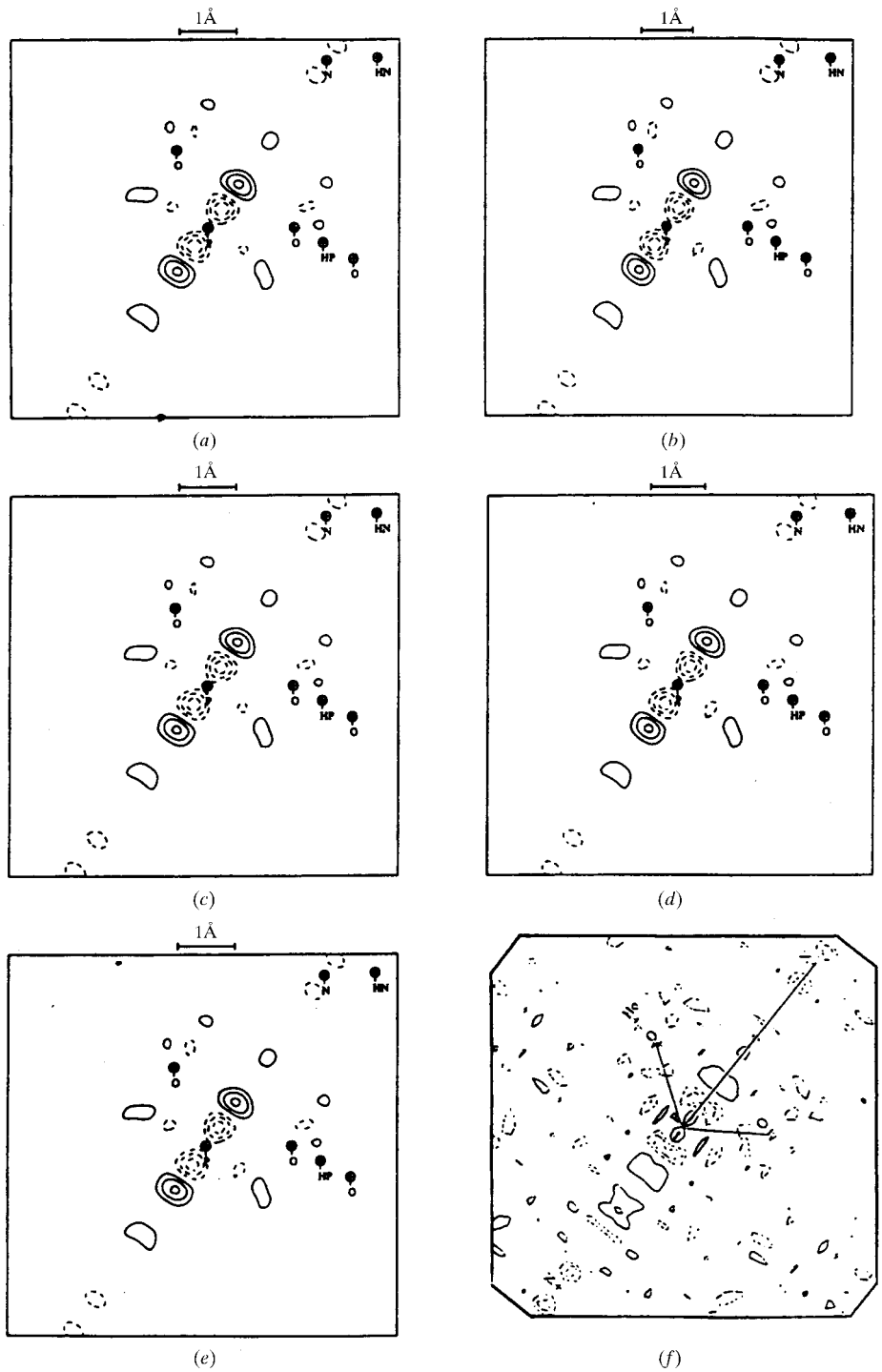

Fig. 2. Residual Fourier maps obtained in the OPO plane (contours of 0.05 e $\AA^{-3}$, full line: positive values; dotted line: negative values), corresponding to: (*a*) $X-(X+N)$ nonconstrained refinement; (*b*), (*c*), (*d*), (*e*) $X-(X+N)$ constrained refinements with net charge of the NH_4 group taken as 0.3, 0.5, 0.7 and 1.0, respectively; (*f*) $X-X$ nonconstrained refinement (Boukhris, 1995).

(*c*) Steps (*a*) and (*b*) were carried out until convergence.

(*d*) Contraction/expansion κ parameter for the spherical part of the valence-electron density of all atoms.

(*e*) Valence population P_v.

(*f*) Multipole populations P_{lm}.

(*g*) κ' contraction/expansion of the multipolar density.

Owing to the strong correlations between κ, P_v, κ' and P_{lm}, the previous parameters were successively refined and the steps from (*d*) to (*g*) were cycled until convergence was reached.

2.3.1. *Charge of the ammonium ion*. The definition of atomic charges in molecules and condensed matter is not unambiguous because it is not a measurable quantity like electron density or electrostatic potential. In fact,

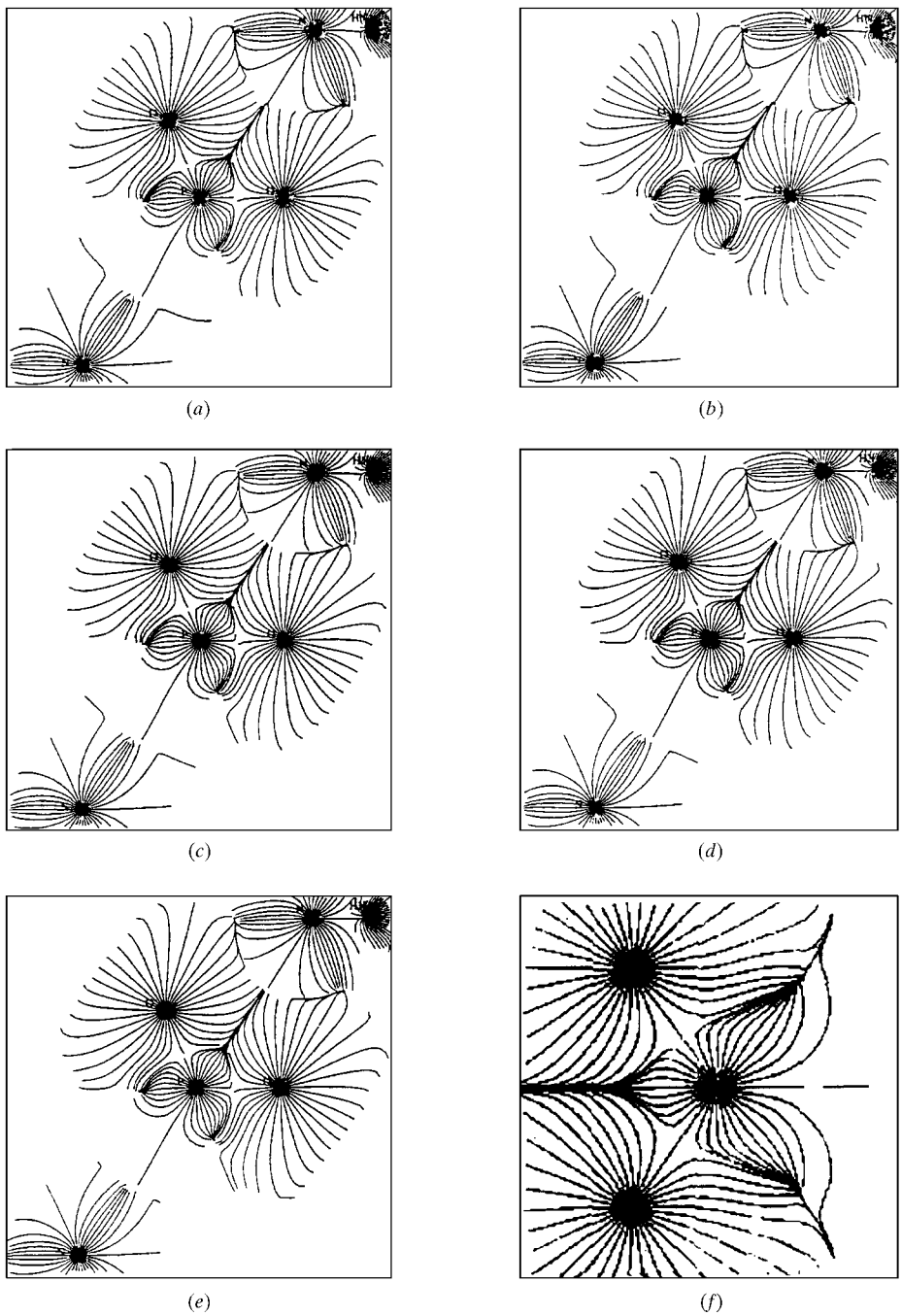

Fig. 3. The gradient vector field of the electron density in the OPO plane corresponding to the refinements as in Fig. 2.

atomic charges are simple quantities in only a formal conceptual sense. They are not directly observable but must be obtained indirectly. Theoretically, they can be derived by Mulliken analysis of molecular orbital populations, by fitting nuclear-centred point charges to molecular electrostatic potential distributions (Bayly *et al.*, 1993) or by volume integration over the topological atomic basin (Bader, 1990) in molecular electron distributions. Experimentally, they can also be derived from X-ray diffraction *via* pseudoatom modelling (Hansen & Coppens, 1978; Coppens *et al.*, 1979), fitting to experimental electrostatic potential (Spackman, 1992; Spackman & Byrom, 1996; Bouhmaida *et al.*, 1997, 1999) or *via* topological analysis (Souhassou & Blessing, 1999). In the present work, the atomic charges are defined from the valence population obtained from the multipolar refinement (1). As the NH_4^+ ion is separated from other ions by a region of very low electron density, we expected the charge of NH_4^+ to be weakly dependent on the definition of atomic charges.

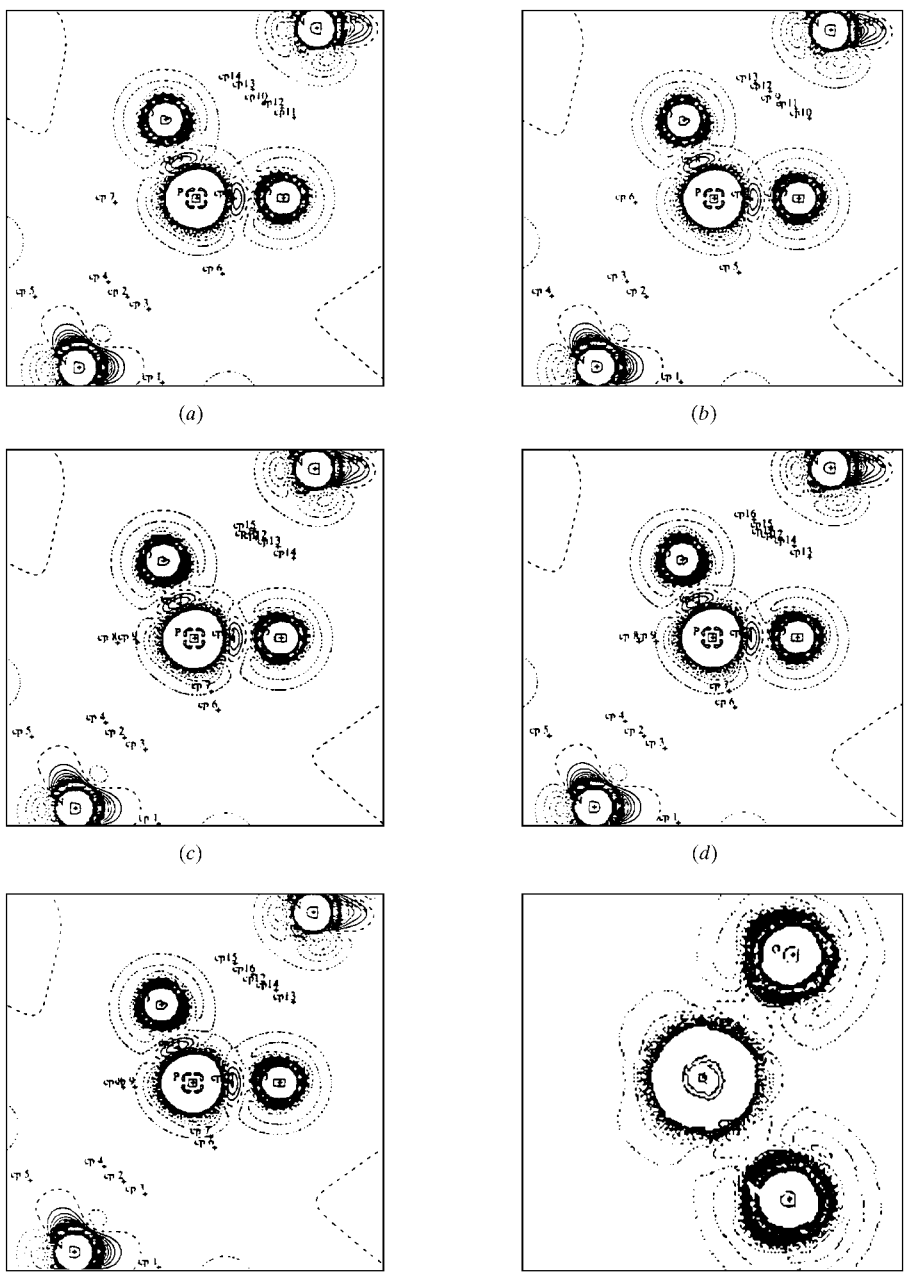

Fig. 4. Maps of the Laplacian of the electron density in the OPO plane (contours 5 e Å^{-5}) corresponding to the same refinements as in Fig. 2.

Table 5. *Topological properties of the electron density at the P–O critical point for different charges of the NH_4 group and comparison with other compounds*

λ_i ($i = 1, 2, 3$) are the eigenvalues of the Hessian matrix. ε is the ellipticity of the electron density at the critical point.

	NH_4 charge	d_1 (Å)	d_2 (Å)	$\lambda_1\ \lambda_2\ \lambda_3$ (e Å^{-5})	$\nabla^2\rho$ (e Å^{-5})	ρ (e Å^{-3})	ε	$\mu = \lambda_1/\lambda_2$	κ'_P
X−*N* study	+0.1 (2)	0.66	0.88	−16.7 −5.3 20.0	−12.0	1.93	0.09	1.31	1.25 (2)
	+0.3	0.66	0.88	−16.8 −15.3 19.5	−12.6	1.94	0.10	1.27	1.26 (2)
	+0.5	0.67	0.88	−16.9 −15.5 18.5	−13.9	1.95	0.09	1.19	1.28 (2)
	+0.7	0.67	0.87	−16.9 −15.5 18.1	−14.4	1.96	0.09	1.17	1.29 (2)
	+1	0.68	0.87	−17.0 −15.6 16.9	−15.7	1.98	0.09	1.08	1.31 (2)
X−*X* study‡		0.64	0.90	−12.3 −11.0 31.7	8.4	1.61	0.11	2.8	1.14 (2)
LAP†	P−O	0.62	0.89	−11.6 −10.94 38.83	16.2	1.68	0.06	3.33	
	P−O(H)	0.64	0.95	−10.61 −8.82 26.35	6.93	1.46	0.20	2.48	

‡ Espinosa *et al.* (1996). † Boukhris (1995).

The above refinement strategy yields a much too small nonspherical charge [+0.1 (2) a.u] for the ammonium ion; the neutrality of the crystal being required, an opposite charge is carried by the H_2PO_4 group. As this charge is very different from the formal charge +1, we made other refinements with constrained charges +0.3, +0.5, +0.7 and finally +1.0 on the ammonium ion. The results, given in Table 3, show that the agreement factors $R(F)$ and $R_w(F)$ as well as the goodness of fit and the scale factor are totally insensitive to the constrained charge. Except for the κ and P_v parameters of the H atoms, the variations of the multipole parameters are not larger than a few e.s.d.'s. Even though we have neutron data for H atoms, the non-uniqueness of the refinement affects only the κ and P_v values of the H atoms (Table 4).

On the other hand, as the protons of the ammonium group are only 0.043 (4) Å from the corresponding NO_nO_{nn} plane (Pérès *et al.*, 1997), one expects a large electron density in this plane and the residual Fourier maps (Fig. 2) provide an additional insight into the quality of the refinements. The residual Fourier map was obtained as:

$$\rho_{\rm res}(\mathbf{r}) = \sum_{\mathbf{H}}{}'(|F_{\rm obs}| - |F_{\rm cal}|)\exp(i\varphi_{\rm cal})\exp(2\pi i\mathbf{H}\cdot\mathbf{r}), \quad (4)$$

where $F_{\rm obs}$ and $F_{\rm cal}$ are the modulus of the observed and calculated structure factors with the multipolar model and $\varphi_{\rm cal}$ the corresponding calculated phase factor. The prime means that the sum is taken over the measured reflections. The maps calculated for all refinements are very similar: the residual electron density does not exceed 0.05 e Å^{-3} and does not show any long-range correlations. The range of the correlations does not exceed one ångström while the resolution of the data is 0.5 Å. Consequently, the charge on the ammonium ion cannot be estimated from the examination of the residual Fourier maps.

In fact, none of the criteria that can be used to check the quality of the different refinements allows the determination of the charge transfer between NH_4 and H_2PO_4. To decide which charge is the more relevant, one has to put into the model some new information: theoretical calculations on the H_2 molecule (Stewart *et al.*, 1965) confirmed by numerous experimental electron densities (Lecomte *et al.*, 1990) show that the κ parameter of the H atoms is close to 1.16. In our refinement, as the κ parameter of the H atom increases from 1 to 1.15 when the charge of NH_4 goes from 0.1 to +1 (Table 4), the charge of +1 a.u. [$\kappa = 1.15\,(2)$] is, as expected, the most appropriate.

2.3.2. *Contraction/expansion of the deformation density of the phosphorus atom*. Let us now consider the topology of the total electron density in the neighbourhood of the (3, −1) critical point of the P−O bond. The maps of the gradient-vector field of the electron density in the OPO plane calculated from *NEWPROP* (Souhassou & Blessing, 1999; Souhassou, 1999) and reported in Fig. 3 are nearly independent of the charge of the ammonium ion: all atomic basins are the same and therefore their integrated properties like net topological charges should be very close. The characteristics of the P−O critical point are given in Table 5 compared with

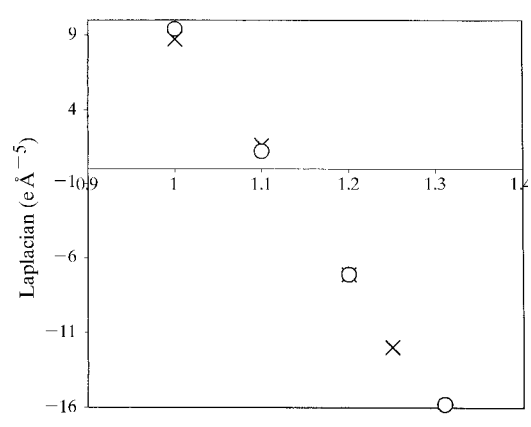

Fig. 5. Laplacian of the electron density at the P−O bond critical point *versus* the contraction parameter κ'_P. Crosses and dots correspond, respectively, to unconstrained and constrained [$q(NH_4) = +1$ a.u] refinements.

Table 6. *Residual indices and multipole parameters for the heavy atoms versus κ'_P when the charge of the NH_4 group is constrained to +1*

		κ'_P			
		1.31	+1.2	+1.1	+1.0
Atom	Parameter				
N	κ	1.009 (3)	1.004 (3)	1.001 (3)	1.002 (3)
	κ'	0.76 (2)	0.72 (1)	0.67 (2)	0.63 (1)
	P_v	1.30 (2)	1.33 (2)	1.35 (2)	1.34 (2)
	P_{20}	−0.001 (7)	−0.002 (8)	0.00 (1)	0.01 (1)
	P_{32+}	0.100 (9)	0.11 (1)	0.12 (1)	0.13 (1)
	P_{32-}	0.16 (3)	0.19 (4)	0.23 (5)	0.26 (6)
	P_{40}	−0.02 (1)	−0.02 (1)	−0.02 (2)	−0.02 (2)
	P_{44+}	0.017 (1)	0.01 (1)	0.00 (2)	−0.01 (2)
	P_{44-}	0.05 (2)	0.06 (2)	0.08 (2)	0.06 (2)
P	κ	1.012 (7)	1.014 (7)	1.016 (7)	1.013 (8)
	P_v	1.11 (3)	1.08 (3)	1.05 (3)	1.01 (3)
	P_{20}	−0.037 (6)	−0.039 (8)	−0.04 (1)	−0.04 (1)
	P_{32+}	0.054 (5)	0.064 (6)	0.076 (7)	0.099 (9)
	P_{32-}	0.20 (3)	0.24 (3)	0.30 (4)	0.36 (5)
	P_{40}	−0.027 (5)	−0.031 (6)	−0.036 (8)	−0.05 (1)
	P_{44+}	−0.010 (4)	−0.013 (5)	−0.019 (7)	−0.027 (9)
	P_{44-}	0.023 (5)	0.032 (6)	0.047 (7)	0.070 (9)
O	κ	0.982 (1)	0.984 (1)	0.987 (1)	0.989 (1)
	κ'	1.18 (5)	1.20 (5)	1.21 (5)	1.19 (5)
	P_v	6.43 (2)	6.37 (2)	6.29 (2)	6.20 (3)
	P_{11+}	−0.007 (4)	−0.011 (4)	−0.015 (4)	−0.020 (5)
	P_{11-}	−0.038 (6)	−0.036 (5)	−0.034 (5)	−0.033 (5)
	P_{10}	−0.029 (4)	−0.030 (5)	−0.030 (5)	−0.030 (5)
	P_{20}	0.010 (4)	0.011 (5)	0.013 (5)	0.014 (5)
	P_{21+}	−0.006 (4)	−0.005 (5)	−0.004 (5)	−0.004 (5)
	P_{21-}	0.012 (6)	0.013 (6)	0.013 (6)	0.014 (6)
	P_{22+}	−0.007 (6)	−0.009 (6)	−0.011 (6)	−0.011 (6)
	P_{22-}	0.014 (5)	0.014 (5)	0.014 (5)	0.013 (5)
	P_{30}	0.003 (6)	0.002 (6)	0.001 (6)	−0.000 (6)
	P_{31+}	−0.017 (7)	−0.021 (7)	−0.025 (7)	−0.030 (7)
	P_{31-}	−0.012 (9)	−0.003 (8)	0.004 (8)	0.011 (8)
	P_{32+}	0.023 (8)	0.015 (8)	0.009 (8)	0.003 (8)
	P_{32-}	0.000 (7)	0.003 (6)	0.005 (6)	0.007 (7)
	P_{33+}	−0.022 (9)	−0.016 (8)	−0.010 (8)	−0.002 (8)
	P_{33-}	−0.020 (6)	−0.023 (6)	−0.025 (6)	−0.027 (6)
H_P	κ	0.93 (2)	0.87 (2)	0.81 (2)	0.75 (1)
	κ'	0.96 (2)	0.97 (3)	0.97 (3)	1.05 (3)
	P_v	0.44 (2)	0.51 (2)	0.60 (3)	0.73 (3)
	P_{11+}	−0.04 (1)	−0.03 (1)	−0.02 (1)	−0.01 (1)
	P_{20}	−0.09 (1)	−0.09 (1)	−0.10 (1)	−0.09 (1)
	P_{21-}	−0.013 (2)	−0.02 (2)	−0.03 (2)	−0.03 (2)
	P_{22+}	−0.29 (3)	−0.28 (3)	−0.27 (3)	−0.22 (2)
H_N	κ	1.15 (2)	1.16 (2)	1.16 (2)	1.15 (2)
	κ'	1.31 (7)	1.47 (8)	1.56 (8)	1.47 (6)
	P_v	0.697	0.666	0.648	0.657
	P_{11+}	0.10 (1)	0.09 (1)	0.09 (1)	0.11 (1)
	P_{11-}	0.00 (1)	−0.00 (1)	−0.01 (1)	−0.01 (1)
	P_{10}	0.04 (3)	0.04 (2)	0.04 (2)	0.05 (2)
	P_{20}	0.01 (2)	0.01 (2)	−0.01 (2)	0.00 (2)
	P_{21+}	0.03 (3)	0.02 (2)	0.02 (2)	0.03 (2)
	P_{21-}	−0.02 (3)	0.01 (2)	0.02 (2)	0.05 (2)
	P_{22+}	0.06 (2)	0.04 (2)	0.03 (2)	0.03 (2)
	P_{22-}	0.02 (2)	0.01 (2)	−0.00 (2)	−0.01 (2)
Scale factor		1.742 (1)	1.742 (1)	1.743 (1)	1.743 (1)
Extinction		1.28 (6)	1.30 (6)	1.31 (6)	1.33 (6)
Residual factors					
$R(F)$ (%)		0.80	0.81	0.81	0.81
$wR(F)$ (%)		0.87	0.87	0.88	0.88
GOF		0.99	0.99	0.99	1.00

other studies of P—O bonds. The electron density at the critical point is nearly independent of the refinement of the charge of the ammonium ion and is consistent with other studies. The most striking feature is the value of the Laplacian of the electron density at the P—O critical point, which is negative while other studies give a slightly positive one. This mainly results from the λ_3 positive eigenvalue of the Hessian matrix which corresponds to the curvature along the bond. By drawing the map of the Laplacian (Fig. 4), one sees that the critical point is located between two regions, where the Laplacian takes opposite signs. As the critical point is closer to phosphorus than to oxygen, we expect the κ'_P parameter of phosphorus to be very relevant. We have consequently performed other refinements with κ'_P values constrained to 1.0, 1.1, 1.2 and 1.31 ($\xi = 3.60$, 3.96, 4.3 and 4.72 Bohr^{-1}) with a charge +1 a.u. for the NH_4 ion. The results reported in Table 6 show that the differences between the agreement factors are not statistically significant. Most parameter variations are not bigger than $\pm 3\sigma$; they are mainly related to the multipole populations of phosphorus and oxygen atoms. These variations are correlated to κ'_P and contribute greatly to the characteristics of the critical point, especially to ∇^2, which is a second derivative and therefore difficult to estimate; the Laplacian, electron density and distance of the critical point from the phosphorus atom are plotted *versus* κ'_P in Figs. 5, 6(*a*) and 6(*b*), respectively. Whereas the Laplacian decreases strongly, the electron density and the distance increase when κ'_P increases. Therefore, as for the NH_4 charge, the diffraction data yields different solutions with the same statistical quality. In that case, however, no additional new information can be added contrary to the charge problem discussed above.

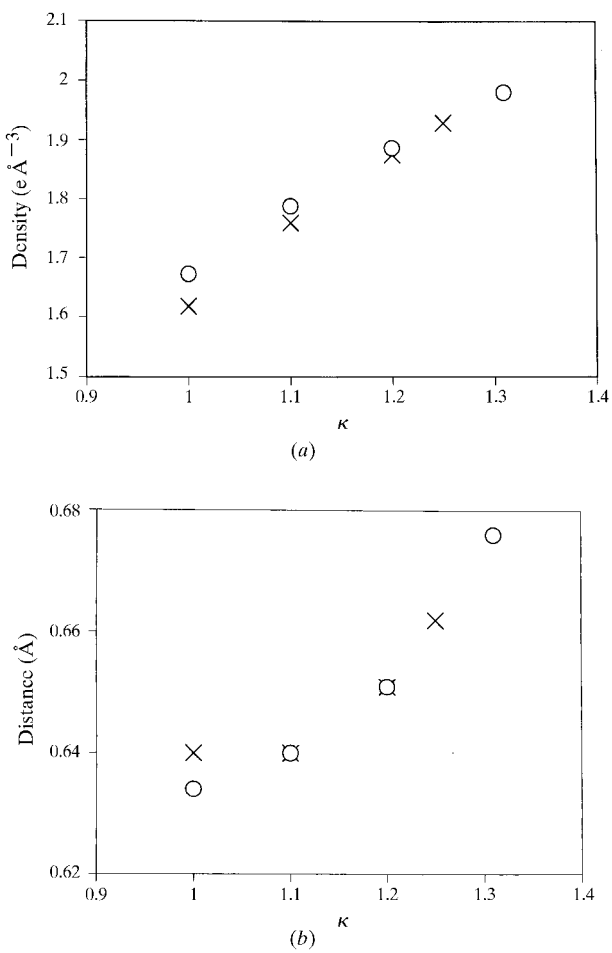

Fig. 6. (*a*) Electron density in the P—O bond critical point *versus* the contraction parameter κ'_P. (*b*) Distance between phosphorus and the P—O bond critical point *versus* the contraction parameter κ'_P. Crosses and dots correspond, respectively, to unconstrained and constrained [$q(NH_4) = +1$ a.u] charge refinements.

3. Conclusions

We show in this paper that several multipole expansions fit the data equally well, and that neither the usual agreement factors nor the residual Fourier maps allow the choice of the physical solution. From a local point of view, the electron density itself slightly depends on the refinement strategy and often the variation among the different solutions does not exceed a few e.s.d.'s. On the contrary, the derivatives of the electron density and mainly the Laplacian at the bond critical points may greatly vary from one solution to another especially for critical points of bonds linking first- and second-row atoms where the charge-density slope is large. Therefore, a few errors in positioning the critical point leads to a large error in $\nabla^2\rho$. This inaccuracy in ∇^2 is also observed in theoretical calculations where the results strongly depend on the quality of the basis set. Therefore, energetics on these covalent bonds calculated from the virial theorem (Bader, 1990) have to be used with great caution. This problem is, however, not a general problem: it does not show up for intermolecular interactions, *i.e.* in regions where ρ and $\nabla\rho$ are small (see for example Espinosa *et al.*, 1999). Further work in this direction is under way.

References

Bader, R. F. W. (1990). *Atoms in Molecules – a Quantum Theory*. Oxford: Clarendon Press.

Bayly, C. I., Cieplak, P., Cornell, W. D. & Kollman, P. A. (1993). *J. Phys. Chem.* **97**, 10269–10280.

Blessing, R. H. (1987). *Crystallogr. Rev.* **1**, 3–58.

Bouhmaida, N., Ghermani, N. E., Lecomte, C. & Thalal, A. (1997). *Acta Cryst.* A**53**, 556–563.

Bouhmaida, N., Ghermani, N. E., Lecomte, C. & Thalal, A. (1999). *Acta Cryst.* A**55**, 729–738.

Boukhris, A. (1995). Thesis, University of Marrakech, Morocco.
Boukhris, A., Lecomte, C., Wyncke, B., Bréhat, F. & Thalal, A. (1994). *J. Phys. Condens. Matter*, **6**, 2475–2488.
Boukhris, A., Souhassou, M., Lecomte, C., Wyncke, B. & Thalal, A. (1998). *J. Phys. Condens. Matter*, **10**, 1621–1641.
Coppens, P., Guru Row, T. N., Leung, P., Stevens, E. D., Becker, P. J. & Yang, Y. W. (1979). *Acta Cryst.* A**35**, 63–72.
De Titta, G. (1985). *J. Appl. Cryst.* **18**, 75–79.
El Haouzi, A., Hansen, N. K., Le Henaff, C. & Protas, J. (1996). *Acta Cryst.* A**52**, 291.
Espinosa, E., Lecomte, C., Molins, E., Ventimillas, A., Cousson, A. & Paulus, W. (1996). *Acta Cryst.* B**52**, 519–534.
Espinosa, E., Souhassou, M., Lachekar, H. & Lecomte, C. (1999). *Acta Cryst.* B**55**, 563–572.
Hansen, N. K. & Coppens, P. (1978). *Acta Cryst.* A**34**, 909–929.
Keeling, R. O. & Pepinsky, R. (1955). *Z. Kristallogr.* **106**, 236–265.
Kuntzinger, S., Ghermani, N. E., Lecomte, C. & Dusausoy, Y. (1998). *Acta Cryst.* B**54**, 819–833.
Lecomte, C., Souhassou, M., Ghermani, N. E., Pichon-Pesme, V. & Bouhmaida, N. (1990). *Trans. Am. Crystallogr. Assoc.* **26**, 55–78.
Moss, G. R., Souhassou, M., Blessing, R. H., Espinosa, E. & Lecomte, C. (1995). *Acta Cryst.* B**51**, 650–660.
Pérès, N., Souhassou, M., Wyncke, B., Gavoille, G., Cousson, A. & Paulus, W. (1997). *J. Phys. Condens. Matter*, **9**, 6555–6562.
Prince, E. & Boggs, P. T. (1992). *International Tables for Crystallography*, Vol. C, edited by A. J. C. Wilson, p. 594. Dordrecht: Kluwer Academic Publishers.
Roversi, P., Irwin, J. J. & Bricogne, G. (1998). *Acta Cryst.* A**54**, 971–996.
Souhassou, M. (1999). *NewProp: Computer Program to Calculate the Topological Properties of Electron Density*. Internal Report CNRS ESA 7036, UHP, Nancy, France.
Souhassou, M. & Blessing, R. H. (1999). *J. Appl. Cryst.* **32**, 210–217.
Souhassou, M., Espinosa, E., Lecomte, C. & Blessing, R. H. (1995). *Acta Cryst.* B**51**, 661–668.
Spackman, M. A. (1992). *Chem. Rev.* **92**, 1769–1797.
Spackman, M. A. & Byrom, P. G. (1996). *Acta Cryst.* B**52**, 1023–1035.
Stewart, R. F. (1969). *J. Chem. Phys.* **51**, 4569–4577.
Stewart, R. F., Davidson, E. R. & Simpson, W. T. (1965). *J. Chem. Phys.* **42**, 175–187.